Drug loading to mesoporous silica carriers by solvent evaporation: A comparative study of amorphization capacity and release kinetics

Marek Šoltys[1,2,3], David Zůza[1], Tereza Boleslavská[1,2], Sarah Akhlasová[1,2], Martin Balouch[1,2], Pavel Kovačík[2], Josef Beránek[2], Nataša Škalko-Basnet[3], Gøril Eide Flaten[3], František Štěpánek[1,*]

[1] Department of Chemical Engineering, University of Chemistry and Technology, Prague, Technická 5, 166 28 Prague 6, Czech Republic

[2] Zentiva, k.s., U Kabelovny 130, 102 00 Praha 10, Czech Republic

[3] Department of Pharmacy, UiT The Arctic University of Norway, Norway

[*] Corresponding author. E-mail: Frantisek.Stepanek@vscht.cz; Tel.:+420 220 443 236.

Abstract

The sorption of poorly aqueous soluble active pharmaceutical ingredients (API) to mesoporous silica carriers is an increasingly common formulation strategy for dissolution rate enhancement for this challenging group of substances. However, the success of this approach for a particular API depends on an array of factors including the properties of the porous carrier, the loading method, or the attempted mass fraction of the API. At present, there is no established methodology for the rational selection of these parameters. In the present work, we report a systematic comparison of four well-characterised silica carriers and seven APIs loaded by the same solvent evaporation method. In each case, we find the maximum amorphization capacity by x-ray powder diffraction analysis and measure the *in vitro* drug release kinetics. For a selected case, we also demonstrate the potential for bioavailability enhancement by a permeation essay.

Keywords: Mesoporous silica particles, amorphization, dissolution kinetics, evaporation loading.

1 Introduction

Innovation in the field of formulation of poorly water soluble active pharmaceutical ingredients (APIs) continues to be of major interest since there is a predominance of poorly water soluble APIs in the drug development pipelines of pharmaceutical industry. Amorphization proved to be an effective strategy to increase solubility and dissolution rate for BCS class II (poorly soluble) and class IV (poorly soluble and poorly permeable) APIs (Edueng et al., 2017). Specifically the use of mesoporous carriers, such as mesoporous silica particles, is receiving significant attention (Bremmell and Prestidge, 2019; Chaudhari

and Gupte, 2017; Diab et al., 2017; Florek et al., 2017; Mellaerts et al., 2010, 2008b; Mura et al., 2019; O'Shea et al., 2017; Riikonen et al., 2018; Xu et al., 2013).

If the mesopores of the carrier are small enough, it becomes thermodynamically more favourable for an API inside the pore to remain in a disordered rather than crystalline state (Rengarajan et al., 2008). Thus, recrystallization and physical stability are less of an issue, unlike what is the situation with simpler non-porous high surface area carriers (Friedrich et al., 2006) or other methods (Zografi and Newman, 2015) such as amorphous solid dispersions (ASD) in polymers. The large surface area of mesoporous silica materials promises faster dissolution rates compared to other amorphization methods available. Moreover, grades of mesoporous silica particle approved as excipients for oral drug delivery are available commercially ("Grace - Uniquely Functional Excipients," 2020, "Merck - Parteck® SLC (Silica) Excipient," 2020). One disadvantage of silica particles is their finite loading capacity. This makes their use in combination with high-dose APIs impractical since the total mass of the resulting tablet would be too high. Compared to polymer ASDs there is by default no solubilizing polymer present in silica particles, that would retard precipitation of the supersaturated API solution. Thus, for APIs that are prone to fast recrystallization after dissolution, specific polymers needs to be added to the final formulation in order to prevent premature precipitation, otherwise the improvement in bioavailability would be negligible (Lainé et al., 2016).

Various methods of loading APIs into the pores of silica carriers exist. These include the melt, sorption, incipient wetness, supercritical CO_2 and the solvent evaporation methods. Depending on the API and the process requirements, different methods might be suitable. The melt method is suitable when a solvent-free operation is desired or when the API has a very poor solubility in solvents (Genina et al., 2018; Mellaerts et al., 2008a; Mužík et al., 2020; Shen et al., 2017; Wang et al., 2006; Waters et al., 2013). On the other hand, it cannot be used for temperature sensitive APIs. Sorption from a solvent is beneficial due to low energy demands of the process. However, to reach high enough loading values, the API needs to be dissolved at high concentration in a solvent with low polarity (Heikkilä et al., 2007; Limnell et al., 2011; Šoltys et al., 2019). The evaporation methods seem to be the most versatile ones so far. They provide high loadings for any API, but one must take into consideration possible recrystallization on the surface of the particles in the case of exceeding the pore capacity. The need to evaporate and recover relatively large quantities of volatile organic solvents can further pose a challenge at the industrial scale (He et al., 2017; Hu et al., 2015; Juère et al., 2017; Le et al., 2019; McCarthy et al., 2016).

Even though individual APIs loaded to various silica carriers under specific conditions have been reported in the literature, systematic studies covering a broader set of APIs in a single, consistent dataset are rare. Comparisons of individual studies with each other can be misleading, because many different parameters influence the behaviour of the API-carrier system, such as the pore size, pore ordering, pore volume, specific surface area, particle size, silanol group concentration and surface functionalisation (Florek et al., 2017; Maleki et al., 2017). In order to make the development of new formulations utilizing API on silica particles more effective, the current research should shift from being descriptive to be predictive. In order to predict the loading and dissolution behaviour using computational tools such as machine learning, more consistent datasets of API/silica combinations are needed.

The goal of this work was therefore to systematically compare the performance of four different silica types at evaporation loading of seven different APIs and thus create one consistent dataset. Two commercially available silica excipients (Parteck® SLC 500 and Syloid® 72FP) and two laboratory prepared silica particles (highly porous sub-micron particles and hierarchically porous micro particles) were used. These silica materials differed mainly in their particle size, pore size and pore volume. The APIs were selected to cover both poorly soluble and highly soluble weak basic, neutral and weak acidic compounds. The maximum non-crystalline loading was determined by using X-ray powder diffraction (XRPD) analysis and the dissolution behaviour was measured using the USP II dissolution method. In addition, to simulate the effect of silica formulation on enhanced absorption in the gastrointestinal tract, an *in vitro* phospholipid vesicle-based permeation assay (PVPA, (Fischer et al., 2011; Flaten et al., 2006)) was conducted with apixaban.

2 Methods

2.1 Materials

Hexadecyltrimethylammonium bromide (CTAB, >99%), tetraethyl orthosilicate (TEOS, >99%), octylamine (OA, >99%) and ammonium hydroxide solution (28-30%) were purchased from Merck. Acetone (p.a.), chloroform ($CHCl_3$, p.a. stabilised by 1% ethanol), dichloromethane (DCM, p.a.), ethanol (for UV spectroscopy), potassium bromide (KBr, for infrared spectroscopy) and isopropanol (p.a.) were purchased from Penta. FaSSIF (Fasted State Simulated Intestinal Fluid powder) was purchased from Biorelevant.com Ltd. Deionized water (Aqual 25, 0.08 µS/cm) was used for all reactions and treatment processes.

Phosphate buffered saline (PBS) at pH 6.8 was prepared by dissolving 6.80 g of KH_2PO_4, 0.94 g of NaOH in 1 l of water. After complete dissolution, the pH was adjusted to 6.85 using HCl (10% v/v) or NaOH (10% w/v).

All APIs (apixaban, amlodipine, ibuprofen, ezetimibe, deferasirox, lacosamide and valsartan) and Syloid® 72FP (72FP), Grace, were kindly provided by Zentiva k.s. (Czech Republic). A sample of Merck Parteck® SLC 500 (SLC 500) was kindly provided by Merck spol. s.r.o. (Czech Republic). Egg phospholipids with 80% phosphatidylcholine (Lipoid E 80) were kindly provided by Lipoid AG (Switzerland).

Silica sub-micron particles (Si-N) and hierarchically porous microparticles (Si-M) were prepared in-house as described below.

2.2 Silica synthesis

Mesoporous sub-micron silica particles (Si-N) were prepared by a soft-templating method reported in our recent work (Šoltys et al., 2019). For one production batch, 1000 ml of water was mixed with 590 ml of ethanol, followed by the addition of 19.6 ml of TEOS and 3.2 g of CTAB. Then 19.6 ml of ammonia solution (28-30 wt% NH_3 in water) was added and the mixture was stirred using an overhead stirrer for 3 hours at room temperature. The suspension was then filtered and washed with ethanol and water. The silica particles were dried and calcined at 600 °C for 6 hours. A typical yield from a single batch was 4.2 g of silica (81 % of theoretical yield).

Hierarchically porous silica microparticles (Si-M) were prepared by an emulsion method as described previously (Zůza et al., 2019). In short, 10 ml of octylamine was mixed with 10 ml of TEOS and the mixture was stirred for 3 min. Then 100 ml of water mixed with 30 ml of ethanol was rapidly added to the mixture and stirred for 3 min. The resulting particles were filtered, washed with ethanol and water, and calcined at 600 °C for 6 hours. A typical yield from a single batch was 2.4 g of silica (88 % of theoretical yield).

The particle size distribution was measured by dynamic light scattering (Microtrac Nano-Flex) and static light scattering (SLS) using Horiba Partica LA-950S2 in the wet dispersion mode (the dispersion media was ethanol), using the batch measurement cuvette. The particle morphology was observed by scanning electron microscopy (SEM Jeol JCM-5700) and transmission electron microscopy (Jeol JEM-1010 TEM microscope). The samples for TEM were sonicated (30W, Bandelin SONOPULS HD 3100) in ethanol for 15 s prior the analysis. The dispersion was then deposited onto carbon-coated copper grids for 5–10 min. Excess of the solution was removed and the grids were dried by Whatman filtration paper. The samples

were observed at an acceleration voltage of 80 kV. The pore size distribution, specific surface area and specific pore volume were evaluated from nitrogen sorption measurements (ASAP 2020, Micromeritics, USA).

2.3 Evaporation loading

In order to load an API into the silica particles, a solution of the the API was first prepared in a solvent in which good solubility was ensured (Šoltys et al., 2019), as specified in Table 1. Then a desired amount of silica was placed in a wide 20 ml scintillation vial and the API solution was dosed onto the powder using a glass pipette at a ratio of 1 ml of API solution per 100 mg of silica in a single impregnation cycle (Figure 1). Typically, batches ranging from 100 mg to 1000 mg of silica in a single vial were made. Depending on the API solution concentration the total required API loading, one or more impregnation cycles were conducted (see supplementary material for detailed list of samples prepared Table S 1). After each impregnation cycle the samples were left to dry on a hot plate heated to 60 °C open to the atmosphere. After the last impregnation cycle the samples were dried in a vacuum oven at 65 °C at 50-100 mbar with a nitrogen bleed to remove any residual solvent. The samples prepared are summarized in **Chyba! Nenalezen zdroj odkazů.**.

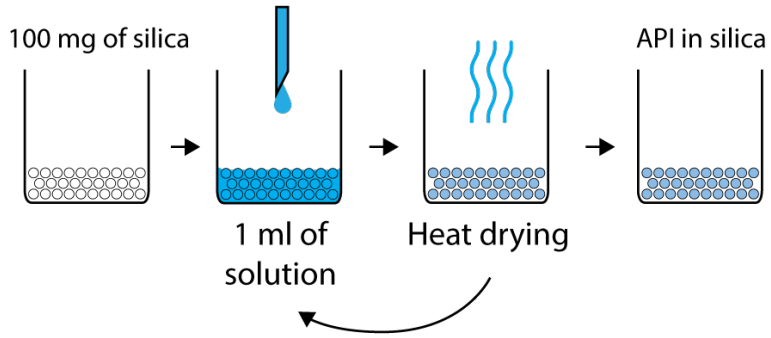

Figure 1: Scheme of the evaporation loading process.

Table 1: Overview of the samples prepared. The values are the relative API loadings (w_{API}/w_{SiO2} x 100). The solvent and API concentration used for evaporation loading are provided in the Supplementary material (Table S 1).

Dissolution rate / functional group	**Weak acids**	**Neutral**	**Weak base**

Fast dissolving	**Ibuprofen** **Si-M:** 10, 30, 50, 60, 70, 80 **Si-N:** 10, 30, 40, 50, 60, 70 **SLC 500:** 10, 30, 50, 60, 70, 80 **72FP:** 10, 30, 50, 70	**Lacosamide** **Si-M:** 20, 40, 60	
Slow dissolving	**Valsartan** **Si-M:** 20, 40, 60 **Deferasirox** **Si-M:** 2.5, 5, 10, 20, 30, 40 **SLC 500:** 20 **72FP:** 20	**Ezetimibe** **Si-M:** 10, 20, 40, 60, 100, 120 **Apixaban** **Si-M:** 10, 30, 40, 50, 60 **SLC 500:** 10, 30, 50 **72FP:** 10, 30, 50	**Amlodipine** **Si-M:** 20, 40, 60

2.4 Characterization of the API state

The physical state of the API after loading (crystalline/amorphous form) was evaluated using XRPD. X-ray powder diffraction data were collected at room temperature with an X'Pert PRO θ-θ powder diffractometer with parafocusing Bragg-Brentano geometry using CuKα radiation (λ = 1.5418 Å, U = 40 kV, I = 30 mA). Data were scanned with an ultrafast detector X'Celerator (or with a scintilator detector equipped with a secondary curved monochromator) over the angular range 5-60° (2θ) with a step size of 0.017° (2θ) and a counting time of 20.32 s step-1. Data evaluation was performed in the software package HighScore Plus 3.0e.

2.5 Dissolution tests

Dissolution experiments were conducted using a USP II dissolution bath (Sotax, Switzerland) coupled to UV-Vis spectrophotometer Specord 200 Plus (Analytic Jena). As the dissolution conditions for individual APIs were set depending on the API solubility and its acido/basic character in order to be discriminative, these are summarized in Table 2. Generally, dissolution experiments were conducted under sink conditions with the exception of ezetimibe (a BSC class II compound that is reported to be almost insoluble in aqueous media). For ezetimibe, dissolution experiments were conducted in the biorelevant media FaSSIF. Peak vessels were used in combination with standard USP II paddle apparatus in order to avoid the coning effect. The media was preheated to 37 °C and stirred at the set agitation speed. The silica samples were

administered as powders. Liquid samples were taken at predefined time-points, filtered through a 0.45 µm filter and analyzed by UV-VIS at an absorption maximum of each API in flow through cuvettes.

Table 2: Dissolution conditions for samples containing different APIs

	API dose (mg)	***Media***	***Volume of media (mL)***	***Apparatus***	***Agitation***	***Quantification wavelength (nm)***
Amlodipine besylate	2	Phosphate buffer, pH 6.8	500	Paddle + peak vessels	75 RPM/45 min; 150 RPM	
Apixaban	2.5	Phosphate buffer, pH 6.8	500	Paddle + peak vessels	75 RPM/45 min; 150 RPM	280
Deferasirox	2.5	Phosphate buffer, pH 6.8	500	Paddle + peak vessels	75 RPM/45 min; 150 RPM	245
Ezetimibe	5	FaSSIF, pH 6.5	500	Paddle + peak vessels	75 RPM/45 min; 150 RPM	232.5
Ibuprofen	10	Phosphate buffer, pH 6.8	150-200	Mini paddles	125 RPM/45 min; 150 RPM	265
Lacosamide	10	Phosphate buffer, pH 6.8	500	Paddle + peak vessels	75 RPM/45 min; 150 RPM	
Valsartan	2.5	Phosphate buffer, pH 6.8	500	Paddle + peak vessels	75 RPM/45 min; 150 RPM	250

2.6 Permeation testing

In order to evaluate the effect of increased API solubility (supersaturation) due to silica formulation on the permeation of the API through the intestinal wall, a phospholipid vesicle-based permeation assay (PVPA) was used (Flaten et al., 2006). The PVPA barriers were prepared according to the method presented by

Flaten, et al. (Flaten et al., 2006). In short, liposomes made from egg phospholipids (Lipoid E 80) were grafted into and onto ester cellulose membranes with pore size of 0.65 µm (in Transwell plate filter inserts – filter area 0.33 cm^2(Corning Inc., New York, USA).), frozen at -80 °C overnight and thawed at 65 °C for 30 min prior use.

Initially experiments with the hydrophilic marker calcein were carried out in order to study the effect of a) the presence of silica particles on the integrity of the barriers and b) the use of FaSSIF in the donor chamber on the integrity of the barriers. In case of a) 2 mg of silica particles were added into the donor together with 200 µl of calcein solution (95.5 mM) in PBS. The acceptor wells were filled with 600 µl of PBS buffer. The permeation experiment was then carried out in the same way as in the original work of Flaten, et al. (Flaten et al., 2006).

In the permeation experiments samples of API loaded in silica (apixaban Si-N 30%) were compared with the same amount of crude API (usually 0.30 mg API in each insert). The samples were weighed into the filter inserts with the PVPA barrier at the bottom (the donor chamber). Once all of the samples were loaded/added, 200 µl of FaSSIF solution was pipetted into the filter inserts and they were placed into the wells (acceptor chamber) of a 24-well plate, which were filled with 600 µl of the same solution. To maintain sink conditions, the filter inserts were moved into a well containing fresh solution at certain time intervals, as shown in Figure 2.

After the assay was finished, the integrity of the barriers was checked by measuring their resistivity using a silver/silver chloride electrode (Millicell ERS-2). If the electrical resistance across the barriers were above the earlier set limit (290 Ohm * cm2) the barriers were regarded intact (Falavigna et al., 2021). Then the API concentration in the acceptor chambers was evaluated using HPLC (Table S 2). The concentration of API in the donor chamber at different times was measured in a separate experiment, since the entire volume of the donor chamber needed to be taken for analysis. For example to measure the donor concentration of apixaban at 6 different time points required the use of 6 barriers, where the first one was measured at 1h, second one at 2h, third one at 3h, etc. Each donor measurement experimental series were performed in triplicate to provide information on reproducibility.

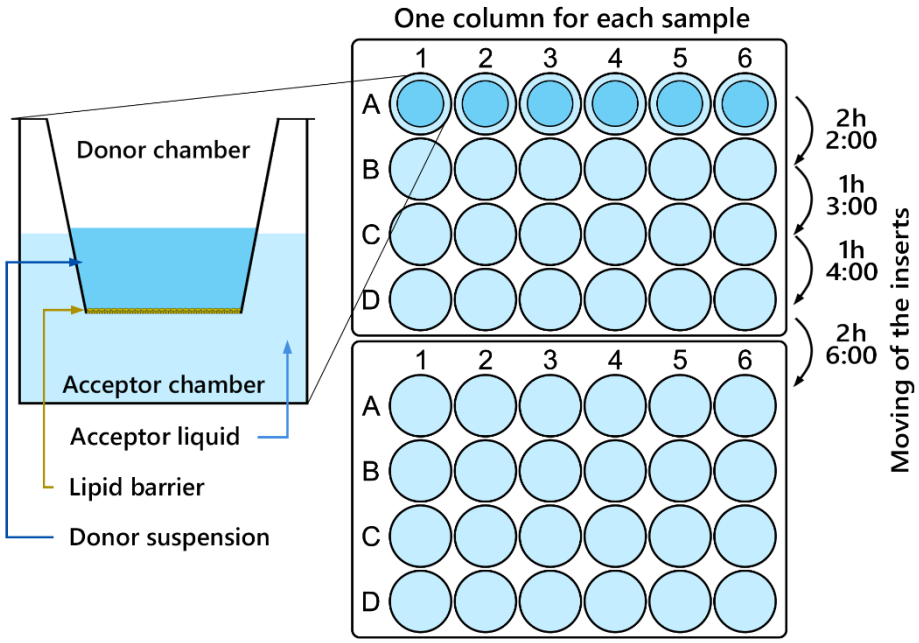

Figure 2: Scheme of the permeation chamber and the experimental setup of the PVPA.

3 Results

3.1 Properties of silica particles

The nitrogen sorption isotherms and the calculated pore size distribution of all four silica materials used in this work are compared in Figure 3 and their main physical and textural properties are summarised in Table 3. The chosen particles differ significantly in the particle size, the pore size distribution, the available pore volume and the total available surface area. The influence of these parameters on the amorphous loading capacity and the dissolution rate was evaluated. SEM images of all four particle types are shown in Figure 4.

a) b)

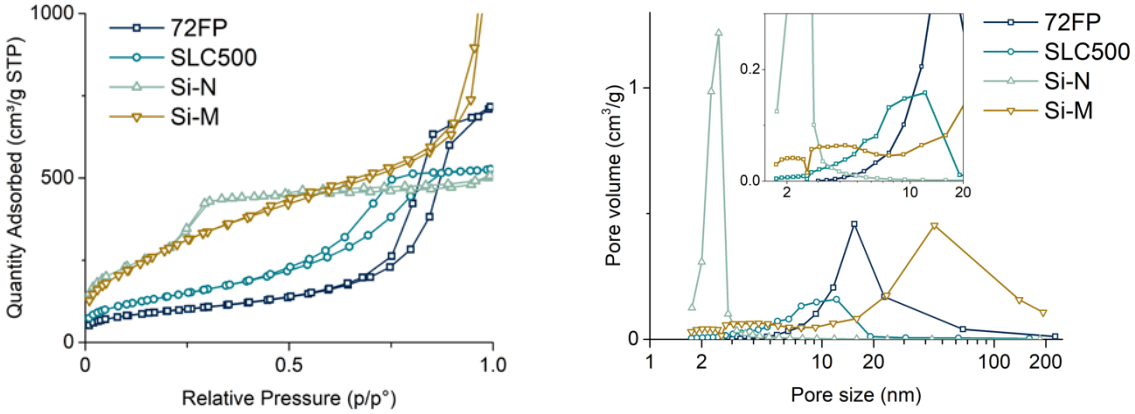

Figure 3: a) The nitrogen sorption isotherms of the four silica samples being compared and b) the pore size distributions.

Table 3: The mean particle size, the specific pore volume, the mean pore diameter, and the specific surface area of silica samples used in this work.

Particles	$\bar{d}_{particle}$ ***(µm)***	V_{pore} ***(cm³/g)***	$\bar{d}_{pore\_BET}$ ***(nm)***	S_{BET} ***(m²/g)***
Si–N	0.6	0.6	2.5	1050
Si–M	35	1.2	4.7	1100
72 FP	6	1.1	12.2	340
SLC 500	11	0.8	6.3	510

a) b)

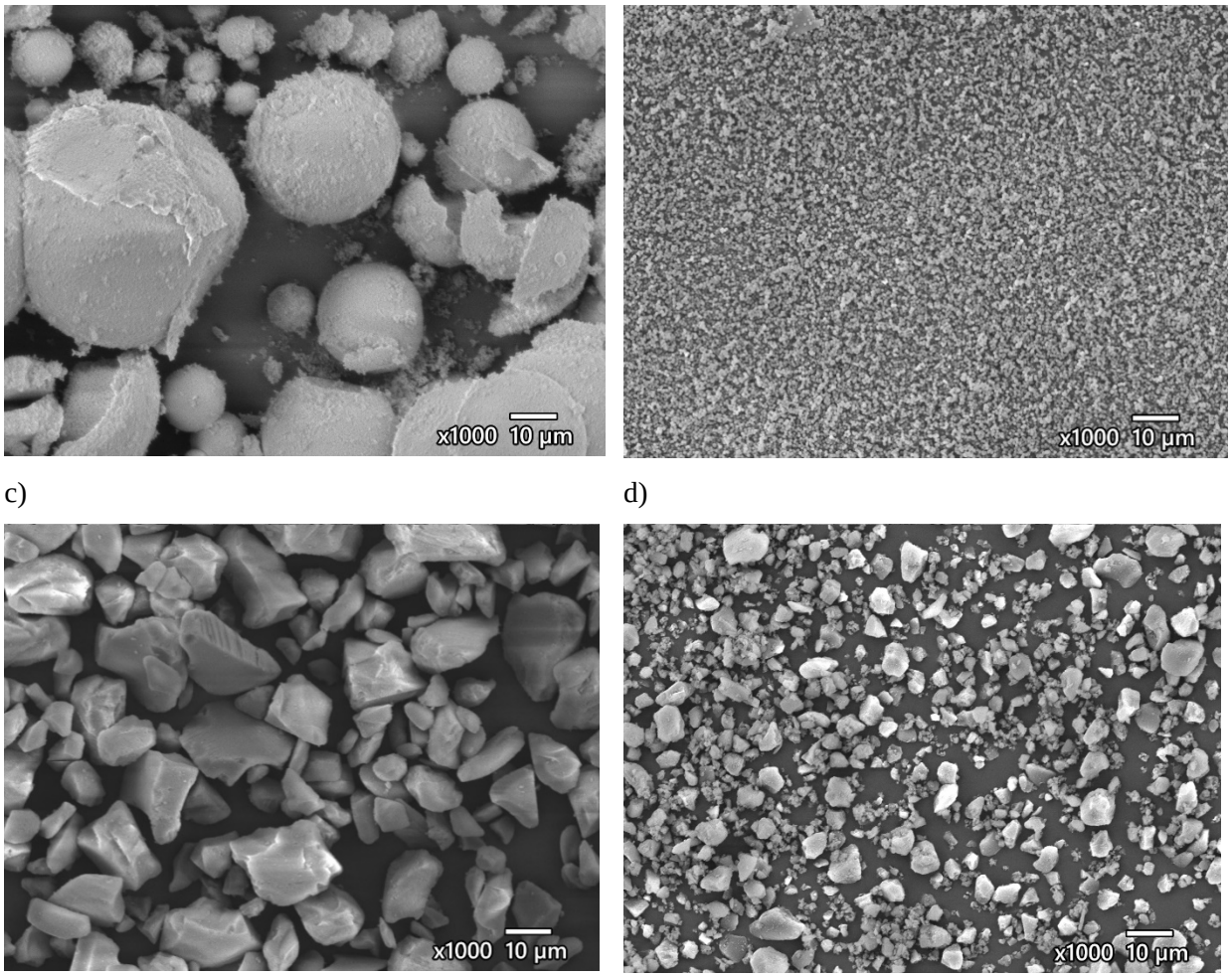

Figure 4: SEM images of the silica particles used. a) Si-M, b) Si-N, c) SLC 500, d) 72 FP

3.2 Amorphous loading capacity of different silica/API combinations

3.2.1 Effect of silica carrier

The total amount of API that can be loaded into the particles in the amorphous form before crystalline phase was observable on the XRPD (amorphous loading capacity) differed for each particle type and also for each API. The particles Si-M had the highest observable amorphous loading capacity in all three of the comparison tests (Figure 5). With apixaban, the sample containing 40 % of apixiban still did not show any crystalline peaks and the sample with 50 % showed only hints of the crystalline phase. On the other hand, the SLC 500 sample showed a significant presence of crystallinity of apixaban at 50 %, and the 72 FP showed the strongest presence of crystalline phase of the three silica particles at the same 50% loading of apixaban (Figure 5A). When ibuprofen was used, the differences between the particles were not as pronounced. Both Si-M and SLC 500 could stabilize 60 % of ibuprofen in the amorphous form, while 80% loading already showed crystallinity. The particles Si-N showed crystallinity at 60% loading of ibuprofen

but no crystallinity was measured at 40% loading. The 72 FP silica exhibited crystallinity already at 30% loading (Figure 5B). With deferasirox, the highest achievable non-crystalline loading was 20 % with Si-M and SLC 500, while the 72 FP sample already showed crystalline presence at this loading (Figure 5C). It is apparent that the combination of high surface area, high pore volume and the pore size in the range of 2 – 10 nm maximizes the amorphous loading capacity. However, in order to get a clear correlation between the texture properties and maximum loading more silica types would need to be tested.

a)

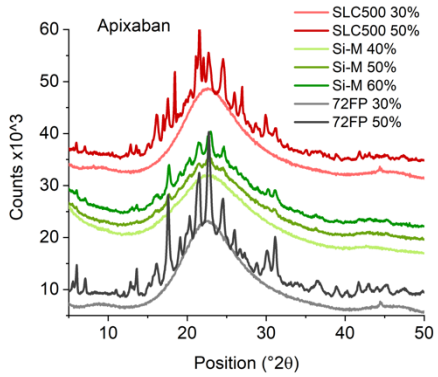

b)

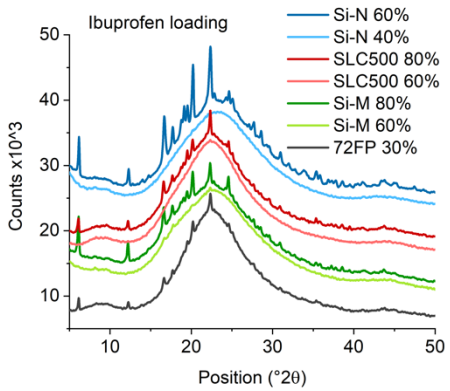

c)

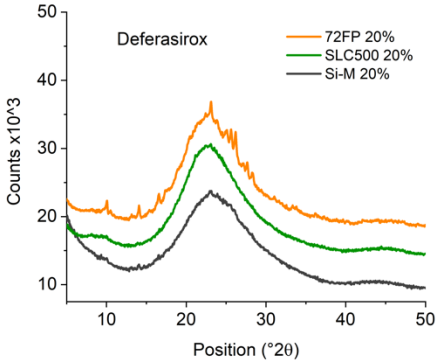

Figure 5: XRPD diffractograms of selected APIs loaded in different types of silica particles. a) apixaban ($CHCl_3$, 2-3 loading cycles), b) loading of ibuprofen (DCM, 2-4 loading cycles), c) loading of deferasirox ($CHCL_3$ + MeOH 3:1, 1 loading cycle).

3.2.2 Effect of API

Since the particles Si-M showed the best performance in all three comparison tests, they were chosen for the screening of the loading capacity of the remaining APIs (Figure 6). The tests with amlodipine, ezetimibe and valsartan did not show any crystalline phase in the XRPD (Figure 6A, C, F). Although with valsartan

this was expected because valsartan does not tend to form the crystalline phase under normal circumstances, it was surprising with amlodipine and ezetimibe. Ezetimibe did not crystallize even at very high loadings, where the theoretical loading capacity given by the free pore volume and the API density was certainly surpassed. With apixaban (Figure 5A), deferasirox, ibuprofen and lacosamide (Figure 6B, D, E) the crystalline phase first appeared at 50 %, 20 %, 70 % and 60 % respectively. With these results, the question about structural connection of API and maximum amorphous loading arises. No simple correlation between maximum amorphous loading and common structural parameters was found (molecular mass, partition coefficient, numbers of hydrogen donors and acceptors, melting temperature or solid density). Even the consideration of Gibbs-Thompson equation for melting depression (Jackson and McKenna, 1990) did not lead to the correlation between structural parameter and maximum amorphous loading. It is important to mention, that the behaviour of only of 7 APIs was observed and for 3 of them no crystalline form was detected. Therefore, it is very easy to make false correlation conclusions from such a small dataset and in order to find correlations purely from experimental results the data set would have to be much larger.

a)

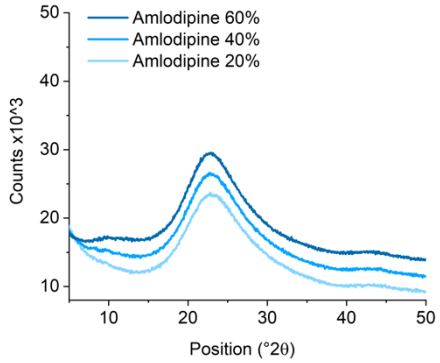

b)

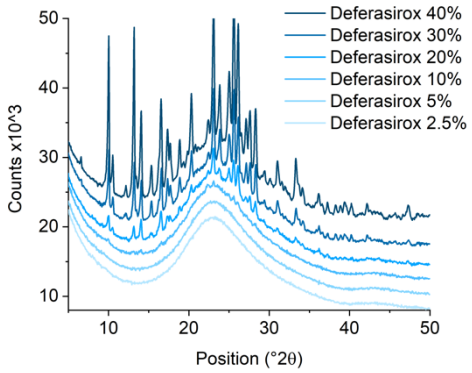

c)

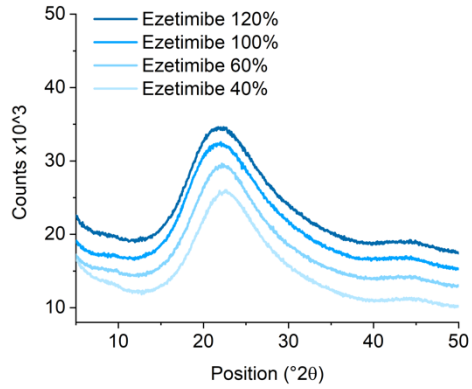

d)

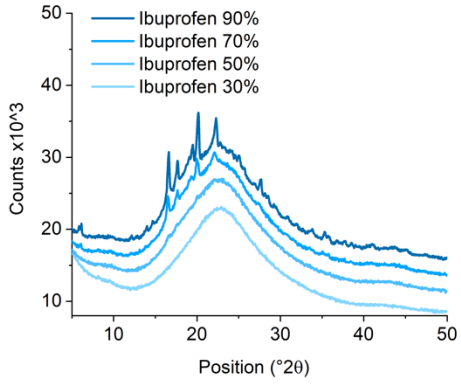

e)

f)

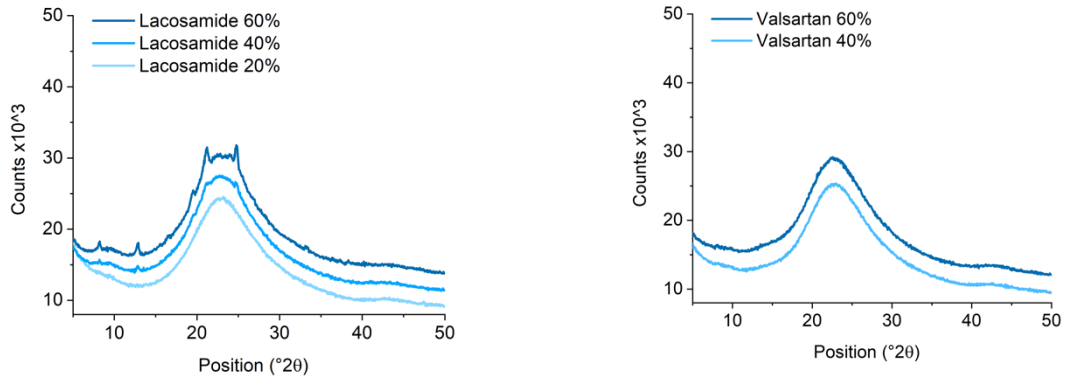

Figure 6: XRPD diffraction patterns of different APIs loaded into the Si-M particles. a) amlodipine, b) deferasirox, c) ezetimibe, d) ibuprofen, e) lacosamide, f) valsartan.

3.2.3 Effect of loading sequence

It was observed that the number of impregnation (loading) cycles conducted can affect the resulting crystallinity of the samples. The outcome of several different loading sequences for the same compound (deferasirox) on the same silica type (Si-M) are summarised in Figure 7. In one case deferasirox was loaded 4 and 8 times by 5 mg/ml solution in isopropanol to prepare 20 % and 40 % loadings respectively. In another case deferasirox was loaded 1 or 2 times using 20 mg/ml solution in a mixture of chloroform and methanol (3:1 v/v) to achieve the same loadings. With an increasing number of cycles the crystallinity increases and appears at lower loadings. The likely mechanism of crystalline phase formation during repeated loading cycles can be understood as follows: during the first loading cycle, an amorphous API is deposited in the silica pores. During the next wetting by the API solution, a supersaturated solution is formed by the partial or full dissolution of the amorphous API into the added solvent. The nucleation of API crystals on the external surface of the silica particles can then take place from this supersaturated solution in parallel with re-deposition of amorphous API inside the pores. During repeated loading/drying cycles, these crystals can serve as secondary nucleation points and the API preferentially deposits on their surface, further exacerbating the overall crystalline content – as seen in the case of 8x isopropanol in Figure 7. This suggests that it is beneficial to use as high API concentration as possible and thus minimise the required number of loading cycles in order to obtain the highest possible amorphous loading capacity.

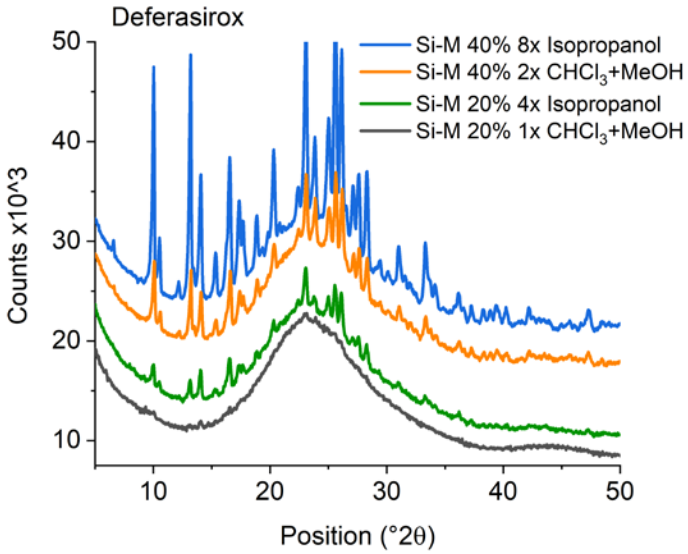

Figure 7: XRPD patterns of four samples of deferasirox loaded into Si-M from isopropanol and chloroform, using different number of loading cycles.

3.3 Dissolution behaviour

3.3.1 Effect of silica carrier

Since the purpose of loading APIs into mesoporous silica particles is to alter their dissolution kinetics, the API/Silica samples were subjected to dissolution tests. The dissolution tests showed significant differences in the dissolution kinetics not only between the different APIs but also for one API loaded on different silica types. All the measured samples were compared to the dissolution kinetics of crude crystalline API as a reference. The most prominent differences were observed in the case of apixaban, shown in Figure 8. All the silica types provided a very fast release when apixaban was present in the amorphous form (10 % and 30 % for Si-M and SLC 500, and 10 % for 72FP). When crystallinity appeared in the sample, the dissolution kinetics slowed down (50 % for Si-M and SLC 500 and >30 % for 72FP). From the dissolution curves it is apparent that the proportional amorphous part dissolved very fast even though the samples contained some crystalline phase. The residual crystalline part of the sample kept dissolving independently of the amorphous one, at approximately the same rate as crude apixaban. However, all of the prepared samples provided faster dissolution than the crude apixaban. This behaviour could potentially be utilized to prepare formulations with combined dissolution rates (e.g. fast on-set of action combined with a more gradual dissolution for longer-term action). To better visualise the difference in dissolution enhancement between the individual samples and the crude API the difference in the dissolved amount from silica sample and from the crude API was plotted vs time in the same graph (Figure 9).

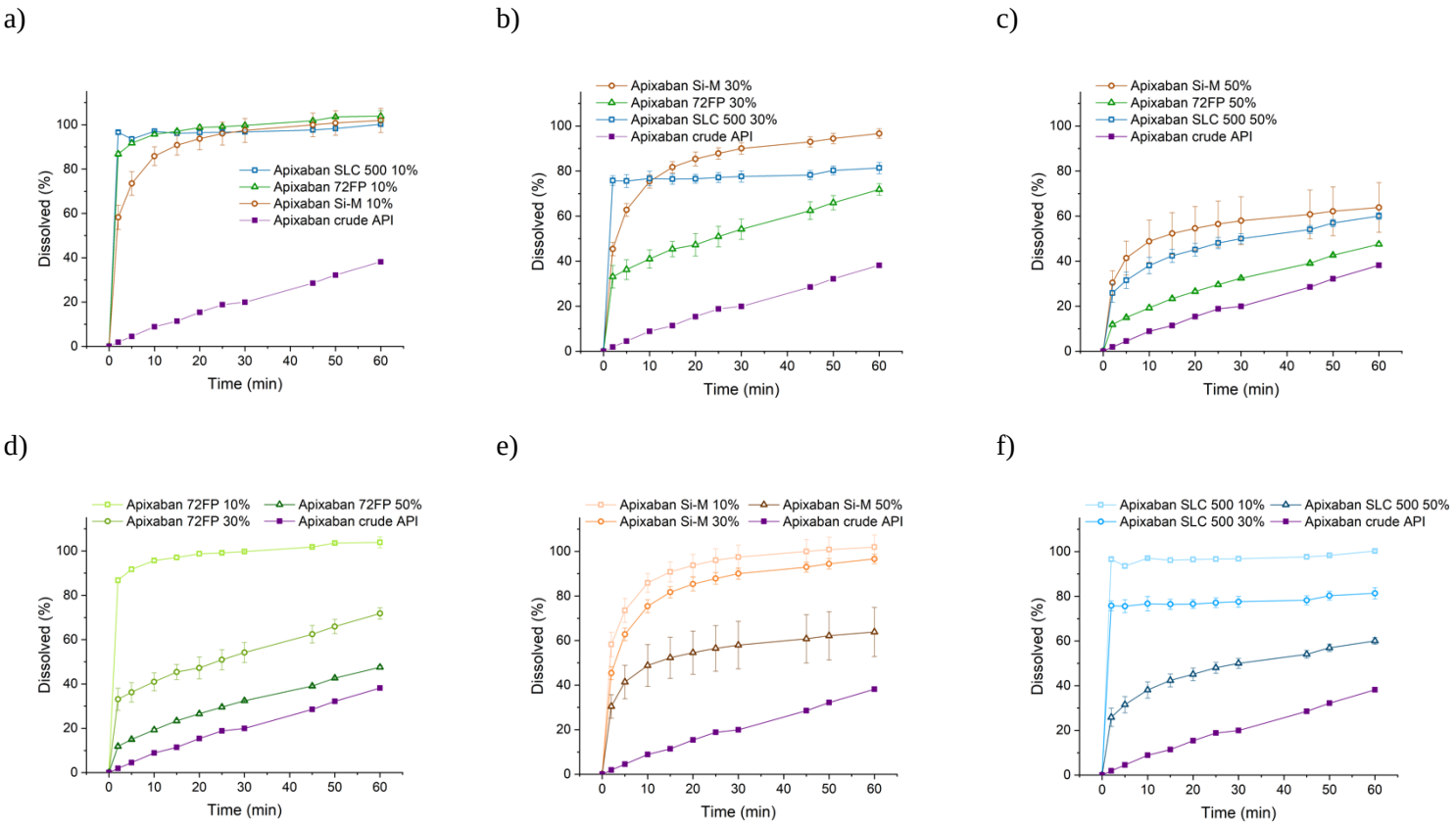

Figure 8: Dissolution kinetics of apixaban samples. Comparison of different silica types at the same loading (a, b, c) and comparison of different loadings in the same silica type (d, e, f).

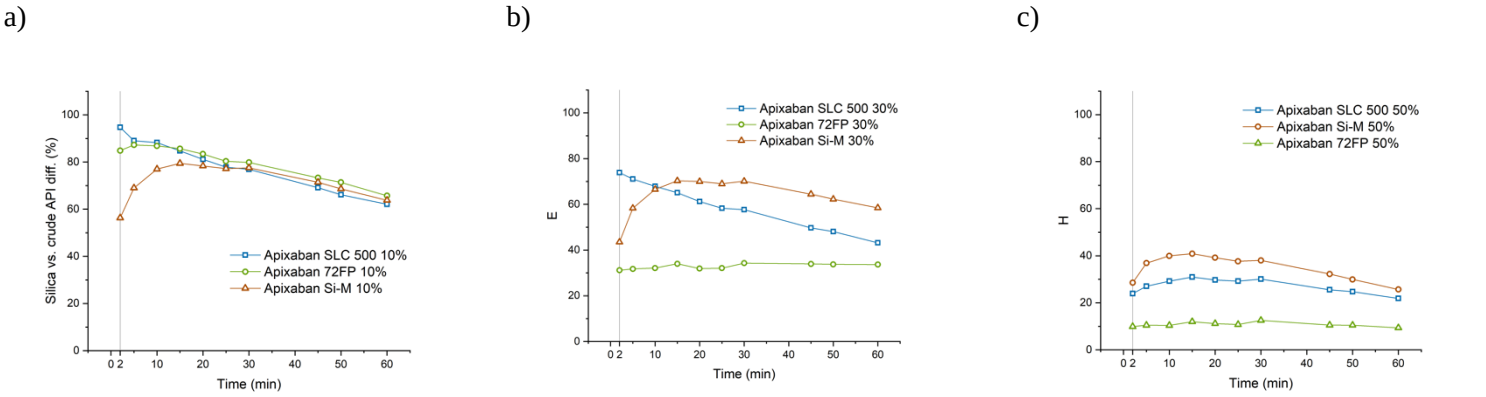

Figure 9: The difference between the dissolved API amount from silica and from the crude form in time for the given samples.

3.3.2 Effect of API

For further API screening only the best-performing Si-M silica particles were used. No differences in dissolution rates were observed with amlodipine, lacosamide and valsartan (Figure 10A, D and E) since the dissolution of crude APIs was already rather fast, even though amlodipine provided incomplete dissolution, which might have been caused by too strong interaction of amlodipine and the silica surface. The dissolved amount increased with higher loading, suggesting a constant amount of the API is bound to the surface and the rest can dissolve. With deferasirox the only sample that provided dissolution enhancement compared to the crude form was the 10% loading, which was the only one fully amorphous. In the case of ezetimibe (Figure 10C), a significant improvement in dissolution rate was achieved. The dissolution rate enhancement was again loading-dependent, and the samples with ≤ 40 % of ezetimibe provided the fastest release. Samples with ibuprofen (Figure 10D) provided burst release when fully amorphous. The 70% sample, which was partially crystalline, had a slower dissolution curve, but was still faster than the crude API.

a)

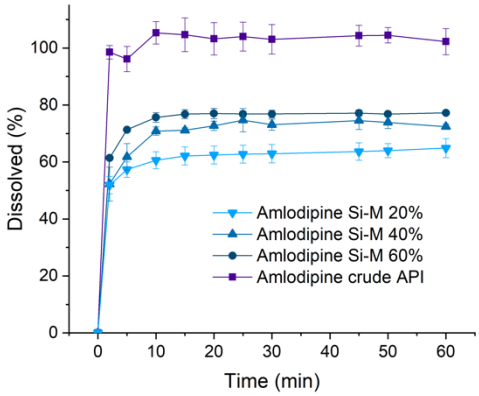

b)

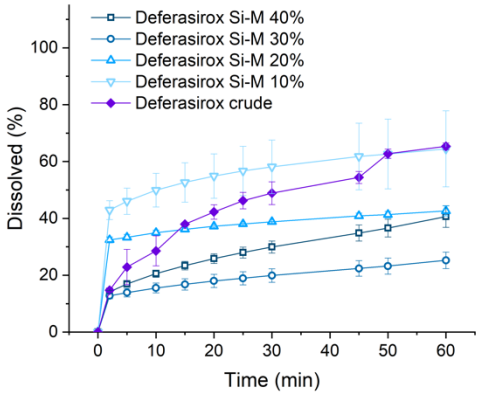

c)

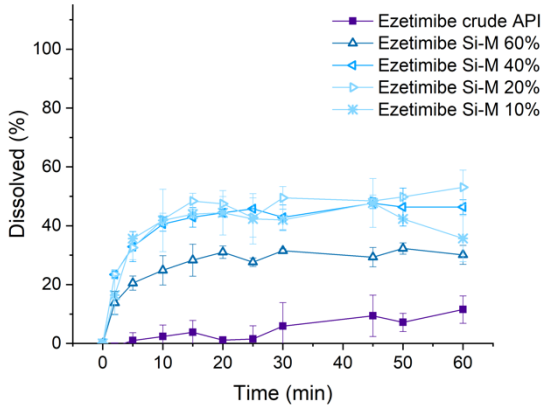

d)

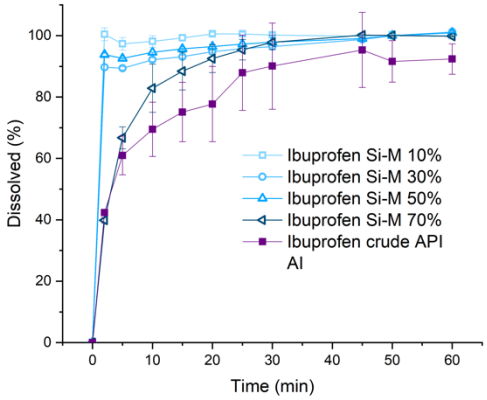

e) f)

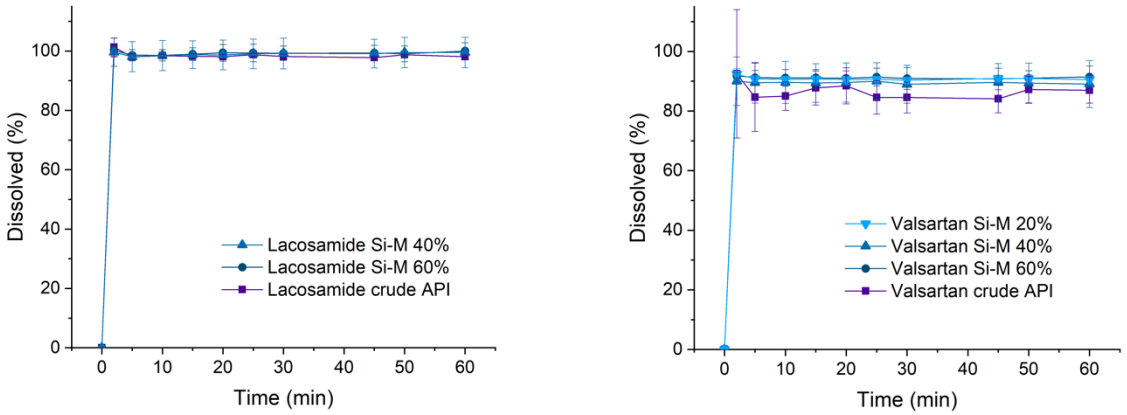

Figure 10: Dissolution kinetics of amlodipine (a), deferasirox (b), ezetimibe (c), ibuprofen (d), lacosamide (e) and valsartan (f) samples loaded in Si-M at various amounts. The weight of each sample being dissolved was always adjusted so the total amount of API inserted was the same for each sample of that particular API (ie 100% dissolved always corresponds to the same API concentration in the dissolution vessel in each graph).

3.4 Permeation test

Under *in vivo* conditions, an increase of API dissolution rate thanks to amorphization would only translate into increased bioavailability if it is matched by increased permeation rate. To simulate this scenario *in vitro*, permeation essays were carried out. Since the permeation experiments with apixaban were conducted using the biorelevant medium FaSSIF, the effect of FaSSIF on the PVPA barrier integrity was tested using the calcein as a model substance (Flaten et al., 2006). The average permeability of calcein in a 6 hour test was 0.026 (± 0.17) $\cdot 10^{-6}$ cm/s, which is below the limit of the reference permeability of calcein in PBS (0.061 $\cdot 10^{-6}$ cm/s (Falavigna et al., 2021; Flaten et al., 2006) and suggests that the FaSSIF does not negatively affect the integrity of the barriers.

Typically, the permeation tests are carried out using concentrated solutions of the APIs in the donor compartments (Fischer et al., 2011). Since in this case the API was inserted in the solid phase in amounts that would cause supersaturation upon full dissolution, the actual concentration of the dissolved API was first measured separately (Figure 11). In the case of apixaban the measured concentration in the donors containing apixaban in silica particles was highest at around 1.5 h into the experiment and reached five to six-fold supersaturation. After that the apixaban started to slowly precipitate, as expected. This caused the concentration to fall over time but despite this, the concentration was still in supersaturation range after 6

h. The concentration in donors containing crude apixaban raised only very slowly and did not even reach the equilibrium solubility concentration at 6 h.

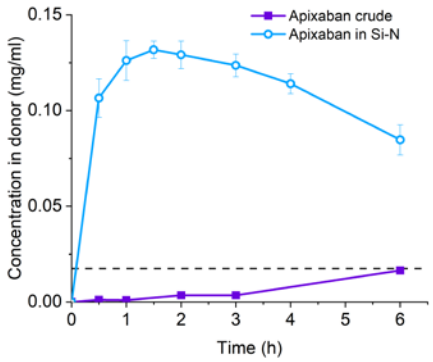

Figure 11: Evolution of the apixaban concentration in the donor phase over time shows strong burst dissolution of the silica loaded apixaban (reaching supersaturation) compared to the crude apixaban. The inserted amount of apixaban into each donor was 0.25 mg, making the theoretical maximum reachable concentration 1.25 mg/ml. The equilibrium solubility of Apixaban in PBS buffer is 0.0175 mg/ml (marked by the dashed line).

The measured concentration in the acceptor compartments was used to calculate the flux of apixaban through the membrane. The flux of apixaban dissolved from silica particles was ten-fold higher than the flux from the crude apixaban samples (Figure 12). Since the concentration in the donor compartment was not constant over time, the otherwise typical steady state of flux, from which the apparent permeability coefficient (P_{app}) is normally calculated, was not reached in this experiment. To get an indication on the estimated in vivo absorption category, the P_{app} was thus calculated as an average of the P_{app} values obtained for the last two data points in Figure 12A for both samples (the P_{app} calculation was done according to Flaten et al. (Flaten et al., 2006), for donor concentration the values of the last two datapoints from Figure 11 were used – see the Supplementary material Table S 3 for details). The averaged values $1.00 \cdot 10^{-6}$ cm/s for crude apixaban and $2.83 \cdot 10^{-6}$ cm/s for apixaban in silica were obtained. The P_{app} values were earlier shown to be directly related to the absorption of drugs *in vivo*, where higher P_{app} signifies higher absorption. For the PVPA model the boundary between moderately absorbing (fraction absorbed ~50%) and well absorbing (fraction absorbed >70%) drugs is at $1.00 \cdot 10^{-6}$ cm/s. This difference as well as the overall higher permeated amount would suggest that the supersaturated concentration can lead to a higher apixaban permeation through the intestinal wall and thus provide higher bioavailability, as was observed in other works for example with fenofibrate loaded in silica administered to pigs (O'Shea et al., 2017) as well as humans (Bukara et al., 2016).

a) b)

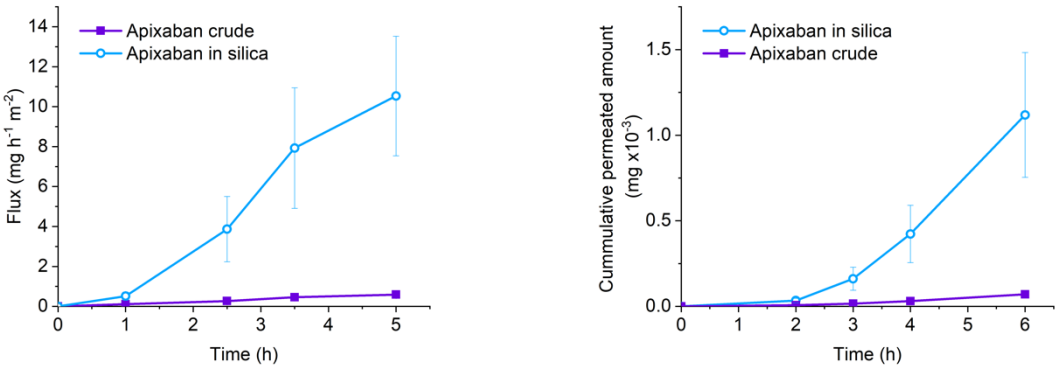

Figure 12: a) The flux of apixaban through the PVPA barriers (calculated from the concentration of apixaban in the acceptor chambers). The results demonstrate that the supersaturation induced in the donor chambers containing the silica formulation increased the flux of apixaban through the barriers. b) The cumulative permeated amount of apixaban from donor to acceptor chamber.

4 Conclusion

This work was concerned with comparing the ability of four structurally different mesoporous silica carriers to incorporate active pharmaceutical ingredients in the amorphous form in order to enhance their dissolution behaviour. It was demonstrated that all seven APIs were successfully loaded into silica particles using the solvent evaporation method at relatively high quantities (≥ 20 % w/w) before crystallization occurred. This was demonstrated also for deferasirox and ezetimibe, which were previously not successfully loaded at high quantities using the sorption method (Šoltys et al., 2019).

Moreover, it was shown that the choice of the silica carrier can have a significant effect not only on the loading capacity, but also on the dissolution kinetics. The key parameter is unsurprisingly the pore size, causing the Syloid® 72FP silica (containing the lowest volume of pores sized below 10 nm) to be the most prone to crystallization after loading. On the other hand, too small pores (2.5 nm) of the Si-N silica can lead to slower initial dissolution even if the samples are fully amorphous. The highest loading was achieved with the Si-M silica, closely followed by Parteck® SLC500. This might suggest that the significantly higher surface area and pore volume of Si-M over the Parteck® SLC 500 silica play only a minor role in the total loading capacity. Compared to the Syloid® 72FP the larger pores (> 20 nm) in the Si-M silica particles do not seem to cause crystallization. The difference is likely caused by the hierarchical porous structure of the Si-M particles (Zůza et al., 2019) due to which the small pores are dried last and thus, unless the capacity of the smaller pores is reached, no deposition causing crystallinity occurs in the larger pores.

The fastest dissolution rates were observed with the Parteck® SLC 500, which, if fully amorphous, always provided a very fast initial burst release (> 80 % of apixaban or ibuprofen dissolved in the first 2 minutes, for ibuprofen data see the supporting information). Interestingly even the samples where crystalline phase was detected using XRPD provided the initial burst release. The amount of API which was released in this manner was lowered proportionally to how much the pore capacity was exceeded and thus, how much of the API was present in the crystalline phase.

Finally, to demonstrate that the silica formulations could provide higher absorption in the gastrointestinal tract (and thus higher bioavailability) a permeation model was used. Apixaban dissolved from silica particles yielded a supersaturated solution, which resulted in a significantly higher flux through the phospholipid barrier (PVPA) compared to apixaban dissolved from its crude form. Over a 6-hour permeation window, the cumulative permeated amount of the apixaban was higher by a factor of 16. The results presented in this work can serve as a methodological guidance for the selection of mesoporous silica carriers along with a loading process in order to formulate poorly soluble APIs. The measurement of amorphous loading capacity by XRPD in combination with *in vitro* dissolution and permeation tests provides a rational basis for identifying formulation prototypes that stand a realistic chance of bioavailability enhancement *in vivo*.

Acknowledgement

F.Š. would like to acknowledge support from the Czech Science Foundation (GAČR project no. 19-26127X). M.Š., D.Z., T.B., S.A., and M.B. would like to thank the Specific University Research (MSMT No 21-SVV/2019). M.Š. would like to thank the support of the Erasmus+ programme of the European Union. The authors would like to thank Dr. Miloslav Lhotka for BET analysis and Ms. Jana Cibulková and Dr. Martina Kohoutková for XPRD measurement. The authors would like to thank Zentiva, k.s., Merck and Lipoid AG for kindly providing materials used in this work.

References

[1] K. Edueng, D. Mahlin, C.A.S. Bergström, The Need for Restructuring the Disordered Science of Amorphous Drug Formulations, Pharm. Res. 34 (2017) 1754–1772. https://doi.org/10.1007/s11095-017-2174-7.

[2] J. Riikonen, W. Xu, V.-P. Lehto, Mesoporous systems for poorly soluble drugs – recent trends, Int. J. Pharm. 536 (2018) 178–186. https://doi.org/https://doi.org/10.1016/j.ijpharm.2017.11.054.

[3] R. Diab, N. Canilho, I.A. Pavel, F.B. Haffner, M. Girardon, A. Pasc, Silica-based systems for oral delivery of drugs, macromolecules and cells, Adv. Colloid Interface Sci. 249 (2017) 346–362. https://doi.org/10.1016/j.cis.2017.04.005.

[4] J.P. O'Shea, K. Nagarsekar, A. Wieber, V. Witt, E. Herbert, C.M. O'Driscoll, C. Saal, D. Lubda, B.T. Griffin, J.B. Dressman, Mesoporous silica-based dosage forms improve bioavailability of poorly soluble drugs in pigs: case example fenofibrate, J. Pharm. Pharmacol. 69 (2017) 1284–1292. https://doi.org/10.1111/jphp.12767.

[5] S. Chaudhari, A. Gupte, Mesoporous Silica as a Carrier for Amorphous Solid Dispersion, Br. J. Pharm. Res. 16 (2017) 1–19. https://doi.org/10.9734/BJPR/2017/33553.

[6] J. Florek, R. Caillard, F. Kleitz, Evaluation of mesoporous silica nanoparticles for oral drug delivery – current status and perspective of MSNs drug carriers, Nanoscale. 9 (2017) 15252–15277. https://doi.org/10.1039/C7NR05762H.

[7] W. Xu, J. Riikonen, V.-P. Lehto, Mesoporous systems for poorly soluble drugs, Int. J. Pharm. 453 (2013) 181–197. https://doi.org/10.1016/j.ijpharm.2012.09.008.

[8] R. Mellaerts, R. Mols, J.A.G. Jammaer, C.A. Aerts, P. Annaert, J. Van Humbeeck, G. Van den Mooter, P. Augustijns, J.A. Martens, Increasing the oral bioavailability of the poorly water soluble drug itraconazole with ordered mesoporous silica, Eur. J. Pharm. Biopharm. 69 (2008) 223–230. https://doi.org/10.1016/j.ejpb.2007.11.006.

[9] R. Mellaerts, K. Houthoofd, K. Elen, H. Chen, M. Van Speybroeck, J. Van Humbeeck, P. Augustijns, J. Mullens, G. Van den Mooter, J.A. Martens, Aging behavior of pharmaceutical formulations of itraconazole on SBA-15 ordered mesoporous silica carrier material, Microporous Mesoporous Mater. 130 (2010) 154–161. https://doi.org/10.1016/j.micromeso.2009.10.026.

[10] K.E. Bremmell, C.A. Prestidge, Enhancing oral bioavailability of poorly soluble drugs with mesoporous silica based systems: opportunities and challenges, Drug Dev. Ind. Pharm. 45 (2019) 349–358. https://doi.org/10.1080/03639045.2018.1542709.

[11] P. Mura, M. Valleri, E. Fabianelli, F. Maestrelli, M. Cirri, Characterization and evaluation of different mesoporous silica kinds as carriers for the development of effective oral dosage forms of glibenclamide, Int. J. Pharm. 563 (2019) 43–52. https://doi.org/10.1016/J.IJPHARM.2019.03.049.

[12] G.T. Rengarajan, D. Enke, M. Steinhart, M. Beiner, Stabilization of the amorphous state of pharmaceuticals in nanopores, J. Mater. Chem. 18 (2008) 2537–2539. https://doi.org/10.1039/B804266G.

[13] H. Friedrich, B. Fussnegger, K. Kolter, R. Bodmeier, Dissolution rate improvement of poorly water-soluble drugs obtained by adsorbing solutions of drugs in hydrophilic solvents onto high surface area carriers, Eur. J. Pharm. Biopharm. 62 (2006) 171–177. https://doi.org/10.1016/j.ejpb.2005.08.013.

[14] G. Zografi, A. Newman, Introduction to Amorphous Solid Dispersions, in: Pharm. Sci. Encycl., John Wiley & Sons, Inc., Hoboken, NJ, USA, 2015: pp. 1–41.

https://doi.org/10.1002/9780470571224.pse522.

[15] Grace - Uniquely Functional Excipients, (2020). https://grace.com/pharma-and-biotech/en-us/formulation-excipients (accessed March 31, 2020).

[16] Merck - Parteck® SLC (Silica) Excipient, (2020). https://www.merckmillipore.com/CZ/cs/products/small-molecule-pharmaceuticals/formulation/solid-dosage-form/parteck-slc/6a2b.qB.ukEAAAFQl6V2h03D,nav (accessed March 31, 2020).

[17] A.-L. Lainé, D. Price, J. Davis, D. Roberts, R. Hudson, K. Back, P. Bungay, N. Flanagan, Enhanced oral delivery of celecoxib via the development of a supersaturable amorphous formulation utilising mesoporous silica and co-loaded HPMCAS, Int. J. Pharm. 512 (2016) 118–125. https://doi.org/10.1016/j.ijpharm.2016.08.034.

[18] L. Wang, F. De Cui, H. Sunada, Preparation and Evaluation of Solid Dispersions of Nitrendipine Prepared with Fine Silica Particles Using the Melt-Mixing Method, Chem. Pharm. Bull. (Tokyo). 54 (2006) 37–43. https://doi.org/10.1248/cpb.54.37.

[19] S.-C. Shen, W.K. Ng, J. Hu, K. Letchmanan, J. Ng, R.B.H. Tan, Solvent-free direct formulation of poorly-soluble drugs to amorphous solid dispersion via melt-absorption, Adv. Powder Technol. 28 (2017) 1316–1324. https://doi.org/https://doi.org/10.1016/j.apt.2017.02.020.

[20] N. Genina, B. Hadi, K. Löbmann, Hot Melt Extrusion as Solvent-Free Technique for a Continuous Manufacturing of Drug-Loaded Mesoporous Silica, J. Pharm. Sci. 107 (2018) 149–155. https://doi.org/10.1016/J.XPHS.2017.05.039.

[21] R. Mellaerts, J.A.G. Jammaer, M. Van Speybroeck, H. Chen, J. Van Humbeeck, P. Augustijns, G. Van den Mooter, J.A. Martens, Physical State of Poorly Water Soluble Therapeutic Molecules Loaded into SBA-15 Ordered Mesoporous Silica Carriers: A Case Study with Itraconazole and Ibuprofen, Langmuir. 24 (2008) 8651–8659. https://doi.org/10.1021/la801161g.

[22] L.J. Waters, T. Hussain, G. Parkes, J.P. Hanrahan, J.M. Tobin, Inclusion of fenofibrate in a series of mesoporous silicas using microwave irradiation, Eur. J. Pharm. Biopharm. 85 (2013) 936–941. https://doi.org/10.1016/J.EJPB.2013.08.002.

[23] J. Mužík, D. Lizoňová, A. Zadražil, F. Štěpánek, Drug amorphisation by fluid bed hot-melt impregnation of mesoporous silica carriers, Chem. Eng. J. 392 (2020) 123754. https://doi.org/10.1016/j.cej.2019.123754.

[24] T. Limnell, H.A. Santos, E. Mäkilä, T. Heikkilä, J. Salonen, D.Y. Murzin, N. Kumar, T. Laaksonen, L. Peltonen, J. Hirvonen, Drug Delivery Formulations of Ordered and Nonordered Mesoporous Silica: Comparison of Three Drug Loading Methods, J. Pharm. Sci. 100 (2011) 3294–3306. https://doi.org/10.1002/jps.22577.

[25] T. Heikkilä, J. Salonen, J. Tuura, N. Kumar, T. Salmi, D.Y. Murzin, M.S. Hamdy, G. Mul, L. Laitinen, A.M. Kaukonen, J. Hirvonen, V.-P. Lehto, Evaluation of Mesoporous TCPSi, MCM-41, SBA-15, and TUD-1 Materials as API Carriers for Oral Drug Delivery, Drug Deliv. 14 (2007) 337–347. https://doi.org/10.1080/10717540601098823.

[26] M. Šoltys, P. Kovačík, O. Dammer, J. Beránek, F. Štěpánek, Effect of solvent selection on drug loading and amorphisation in mesoporous silica particles, Int. J. Pharm. 555 (2019) 19–27. https://doi.org/10.1016/j.ijpharm.2018.10.075.

[27] L. Hu, H. Sun, Q. Zhao, N. Han, L. Bai, Y. Wang, T. Jiang, S. Wang, Multilayer encapsulated mesoporous silica nanospheres as an oral sustained drug delivery system for the poorly water-soluble drug felodipine, Mater. Sci. Eng. C. 47 (2015) 313–324. https://doi.org/10.1016/j.msec.2014.10.067.

[28] E. Juère, J. Florek, M. Bouchoucha, S. Jambhrunkar, K.Y. Wong, A. Popat, F. Kleitz, In Vitro Dissolution, Cellular Membrane Permeability, and Anti-Inflammatory Response of Resveratrol-Encapsulated Mesoporous Silica Nanoparticles, Mol. Pharm. 14 (2017) 4431–4441. https://doi.org/10.1021/acs.molpharmaceut.7b00529.

[29] Y. He, S. Liang, M. Long, H. Xu, Mesoporous silica nanoparticles as potential carriers for enhanced drug solubility of paclitaxel, Mater. Sci. Eng. C. 78 (2017) 12–17. https://doi.org/10.1016/J.MSEC.2017.04.049.

[30] C.A. McCarthy, R.J. Ahern, R. Dontireddy, K.B. Ryan, A.M. Crean, Mesoporous silica formulation strategies for drug dissolution enhancement: a review, Expert Opin. Drug Deliv. 13 (2016) 93–108. https://doi.org/10.1517/17425247.2016.1100165.

[31] T.-T. Le, A.K. Elzhry Elyafi, A.R. Mohammed, A. Al-Khattawi, Delivery of Poorly Soluble Drugs via Mesoporous Silica: Impact of Drug Overloading on Release and Thermal Profiles, Pharmaceutics. 11 (2019) 269. https://doi.org/10.3390/pharmaceutics11060269.

[32] A. Maleki, H. Kettiger, A. Schoubben, J.M. Rosenholm, V. Ambrogi, M. Hamidi, Mesoporous silica materials: From physico-chemical properties to enhanced dissolution of poorly water-soluble drugs, J. Control. Release. 262 (2017) 329–347. https://doi.org/https://doi.org/10.1016/j.jconrel.2017.07.047.

[33] S.M. Fischer, G.E. Flaten, E. Hagesæther, G. Fricker, M. Brandl, In-vitro permeability of poorly water soluble drugs in the phospholipid vesicle-based permeation assay: the influence of nonionic surfactants, J. Pharm. Pharmacol. 63 (2011) 1022–1030. https://doi.org/10.1111/j.2042-7158.2011.01301.x.

[34] G.E. Flaten, A.B. Dhanikula, K. Luthman, M. Brandl, Drug permeability across a phospholipid vesicle based barrier: A novel approach for studying passive diffusion, Eur. J. Pharm. Sci. 27 (2006)

80–90. https://doi.org/10.1016/J.EJPS.2005.08.007.

[35] D. Zůza, M. Šoltys, J. Mužík, D. Lizoňová, M. Lhotka, P. Ulbrich, O. Kašpar, F. Štěpánek, Silica particles with three levels of porosity for efficient melt amorphisation of drugs, Microporous Mesoporous Mater. (2019). https://doi.org/10.1016/j.micromeso.2018.07.033.

[36] M. Falavigna, S. Brurok, M. Klitgaard, G.E. Flaten, Simultaneous assessment of in vitro lipolysis and permeation in the mucus-PVPA model to predict oral absorption of a poorly water soluble drug in SNEDDSs, Int. J. Pharm. 596 (2021) 120258. https://doi.org/10.1016/j.ijpharm.2021.120258.

[37] C.L. Jackson, G.B. McKenna, The melting behavior of organic materials confined in porous solids, J. Chem. Phys. 93 (1990) 9002–9011. https://doi.org/10.1063/1.459240.

[38] K. Bukara, L. Schueller, J. Rosier, M.A. Martens, T. Daems, L. Verheyden, S. Eelen, M. Van Speybroeck, C. Libanati, J.A. Martens, G. Van Den Mooter, F. Frérart, K. Jolling, M. De Gieter, B. Bugarski, F. Kiekens, Ordered mesoporous silica to enhance the bioavailability of poorly water-soluble drugs: Proof of concept in man, Eur. J. Pharm. Biopharm. 108 (2016) 220–225. https://doi.org/10.1016/j.ejpb.2016.08.020.

Supplementary material

Evaporation samples preparation

Table S 1: The table of prepared samples.

Sample	Silica [mg]	Solvent	Solvent volume per cycle [ml]	Concentration [mg/ml]	# of cycles
APX-SiMicro-2.5%	100	$CHCl_3$	1	2.5	1
APX-SiMicro-5%	100	$CHCl_3$	1	5	1
APX-SiMicro-10%	100	$CHCl_3$	1	10	1
APX-SiMicro-20%	100	$CHCl_3$	1	20	1
APX-SiMicro-30%	100	$CHCl_3$	1	10, 20	1, 1
APX-SiMicro-40%	100	$CHCl_3$	1	20	2
APX-SiMicro-50%	100	$CHCl_3$	1	10, 20	1, 2
APX-SiMicro-60%	100	$CHCl_3$	1	20	3
APX-SLC500-2.5%	100	$CHCl_3$	1	2.5	1
APX-SLC500-5%	100	$CHCl_3$	1	5	1
APX-SLC500-10%	100	$CHCl_3$	1	10	1

APX-SLC500-20%	100	$CHCl_3$	1	20	1
APX-SLC500-30%	100	$CHCl_3$	1	10, 20	1, 1
APX-SLC500-50%	100	$CHCl_3$	1	10, 20	1, 2
APX-Syl72FP-2.5%	100	$CHCl_3$	1	2.5	1
APX-Syl72FP-5%	100	$CHCl_3$	1	5	1
APX-Syl72FP-10%	100	$CHCl_3$	1	10	1
APX-Syl72FP-20%	100	$CHCl_3$	1	20	1
APX-Syl72FP-30%	100	$CHCl_3$	1	10, 20	1+1
APX-Syl72FP-50%	100	$CHCl_3$	1	10, 20	1+2
IBU-SiMicro-2%	100	DCM	1	2	11
IBU-SiMicro-5%	100	DCM	1	5	
IBU-SiMicro-10%	100	DCM	1	10	1
IBU-SiMicro-20%	100	DCM	1	20	1
IBU-SiMicro-30%	100	DCM	1	10, 20	1+1
IBU-SiMicro-50%	100	DCM	1	10, 20	1+2
IBU-SiMicro-70%	100	DCM	1	10, 20	1+3
IBU-SiMicro-90%	100	DCM	1	10, 20	1+4
IBU-SiMicro-10%_b	1000	DCM	5	10	2
IBU-SiMicro-30%_b	350	DCM	2, 1.5	30	2
IBU-SiMicro-50%_b	300	DCM	2, 1	50	2
IBU-SiMicro-70%_b	300	DCM	2, 1	70	2
IBU-SLC500-10%	1000	DCM	5	10	2
IBU-SLC500-30%	350	DCM	2, 1.5	30	2
IBU-SLC500-50%	300	DCM	2, 1	50	2
IBU-SLC500-70%	300	DCM	2, 1	70	2
IBU-Syl72FP-10%	1000	DCM	5	10	2
IBU-Syl72FP -30%	350	DCM	2, 1.5	30	2
IBU-Syl72FP -50%	300	DCM	2, 1	50	2
IBU-Syl72FP -70%	300	DCM	2, 1	70	2
IBU-SiNano-10%	900	DCM	5, 4	10	2
IBU-SiNano-30%	350	DCM	2, 1.5	30	2
IBU-SiNano-50%	300	DCM	2, 1	50	2
IBU-SiNano-70%	300	DCM	2, 1	70	2

DEF-SiMicro-20%_1x	100	MeOH+CHCl3 (1:3)	1	20	1
DEF-SiMicro-20%_4x	100	Isopropanol	1	5	4
DEF-SiMicro-40%_2x	100	MeOH+CHCl3 (1:3)	1	20	2
DEF-SiMicro-40%_8x	100	Isopropanol	1	5	8
DEF-SiMicro-2.5%	100	Isopropanol	1	2.5	1
DEF-SiMicro-5%	100	Isopropanol	1	5	1
DEF-SiMicro-10%	100	Isopropanol	1	5	2
DEF-SiMicro-20%	100	Isopropanol	1	5	4
DEF-SiMicro-30%	100	Isopropanol	1	5	6
DEF-SiMicro-40%	100	Isopropanol	1	5	8
AML-SiMicro-5%	100	DCM	1	5	1
AML-SiMicro-10%	100	DCM	1	10	1
AML-SiMicro-20%	100	DCM	1	20	1
AML-SiMicro-40%	100	DCM	1	20	2
AML-SiMicro-60%	100	DCM	1	20	3
LAC-SiMicro-5%	100	DCM	1	5	1
LAC-SiMicro-10%	100	DCM	1	10	1
LAC-SiMicro-20%	100	DCM	1	20	1
LAC-SiMicro-40%	100	DCM	1	20	2
LAC-SiMicro-60%	100	DCM	1	20	3
VAL-SiMicro-5%	100	DCM	1	5	1
VAL-SiMicro-10%	100	DCM	1	10	1
VAL-SiMicro-20%	100	DCM	1	20	1
VAL-SiMicro-40%	100	DCM	1	20	2
VAL-SiMicro-60%	100	DCM	1	20	3
EZE-SiMicro-5%	100	Acetone	1	5	1
EZE-SiMicro-10%	100	Acetone	1	10	1
EZE-SiMicro-20%	100	Acetone	1	20	1
EZE-SiMicro-40%	100	Acetone	1	20	2
EZE-SiMicro-60%	100	Acetone	1	20	3
EZE-SiMicro-100%	100	Acetone	1	20	5

EZE-SiMicro-120%	100	Acetone	1	20	6

HPLC measurement method

The apixaban concentration in the permeation experiments was determined using HPLC with UV detector. A gradient method was used on Waters C18 column (3 µm 150x4.6 mm). The mobile phase consisted of component A (Di-ammonium hydrogen phosphate, 1.32 mg/ml at pH 7.00 ± 0.05 adjusted by phosphoric acid) and component B (Acetonitrile). The flow rate was 0.7 ml/min, the injection volume 10.0 µl, autosampler temperature 25 °C, column temperature 35 °C and the UV wavelength was set to 279 nm.

Table S 2: Gradient program for the HPLC measurement.

Time (min)	**Component A (%)**	**Component B (%)**
0.0	70	30
2.0	20	80
4.0	70	30
7.0	70	30

SEM images of the used particles at lower magnification:

SLC 500:

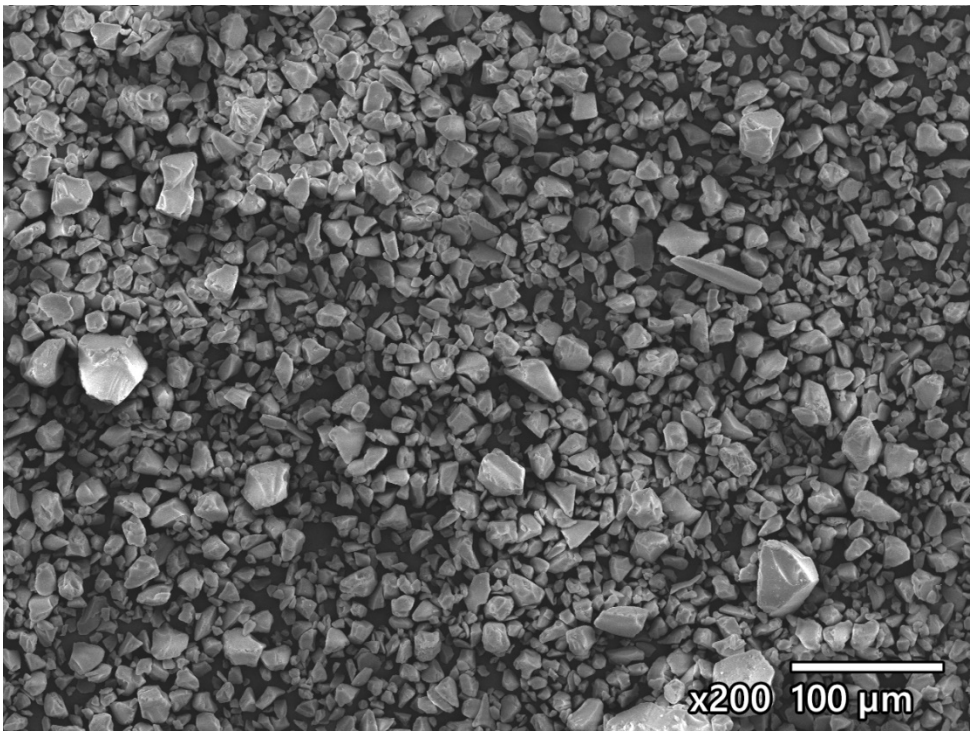

Si-N:

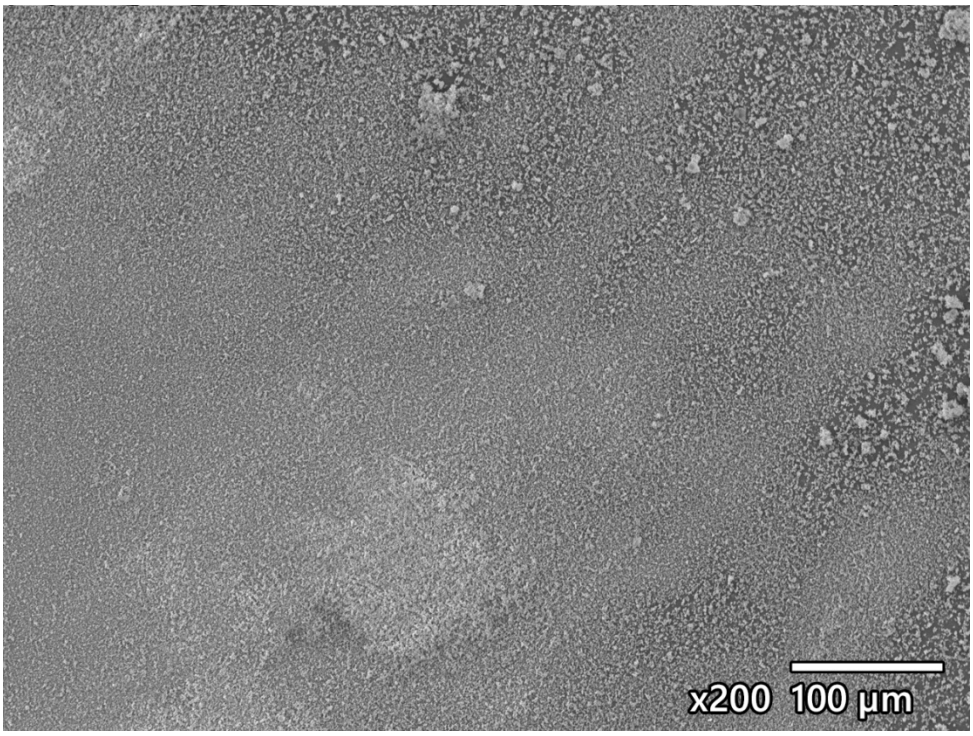

Si-M:

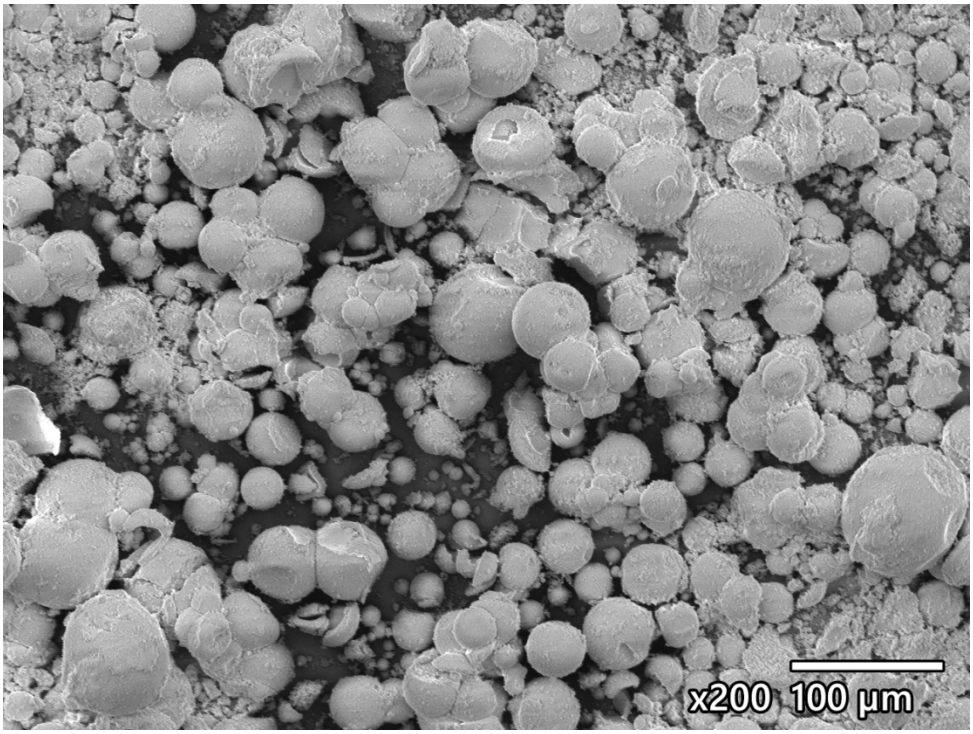

72 FP:

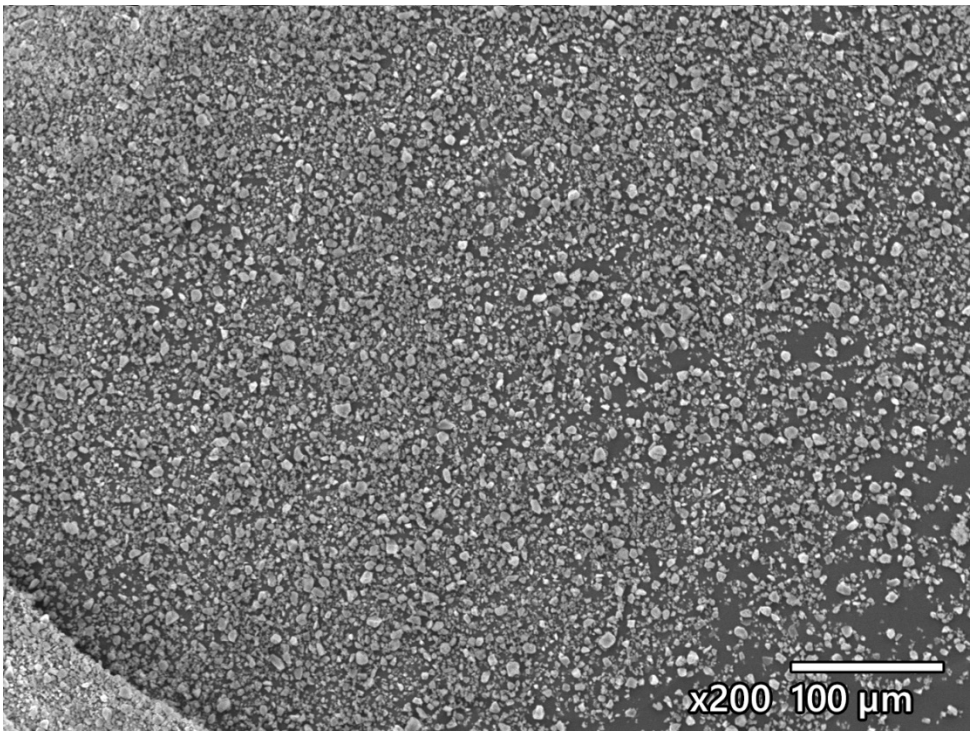

Papp calculation average

Table S 3: Values of P_{app} for individual time-points that were averaged to obtain the final presented value

Apixaban in silica			
Data point	Flux (nmol/s/cm^2)	Donor conc. (nmol/ml)	Papp (cm/s)
4 h	4.79 x10^{-04}	255.0432	1.88 x10^{-06}
6 h	6.37 x10^{-04}	168.1878	3.79 x10^{-06}
P_{app} average			**2.83 x10^{-06}**
Apixaban crude			
4 h	2.76 x10^{-05}	26.7684	1.03 x10^{-06}
6 h	3.56 x10^{-05}	36.4778	9.76 x10^{-07}
P_{app} average			**1.00 x10^{-06}**